Generating oxygen vacancies in Cu^{2+}-doped TiO_2 hollow spheres for enhanced photocatalytic activity and antimicrobial activity

Hongguang Zhang[1] ✉, *Meng Wang*[2], *Feng Xu*[1]

[1]*College of Pharmacy, Qiqihar Medical University, Qiqihar 161006, People's Republic of China*
[2]*College of Adult and Continuing Education, Qiqihar Medical University, Qiqihar 161006, People's Republic of China*
✉ *E-mail: zhanghg@qmu.edu.cn*

Published in Micro & Nano Letters; Received on 15th December 2019; Revised on 16th March 2020; Accepted on 15th April 2020

Developing cheap photocatalysts with highly visible-light activity is greatly desired for environmental pollution treatment. In this work, the authors designed and synthesised Cu^{2+}-doped TiO_2 (Cu-TiO_2) hollow spheres with enhanced photocatalytic activity and antimicrobial activity using a simple hydrothermal process. The X-ray powder diffraction (XRD) results revealed that Cu-TiO_2 hollow spheres were anatase crystal phase. The Cu^{2+}-doped into TiO_2 can be confirmed by XRD, Raman spectra, and UV–Vis spectrum. The photocatalytic activity of Cu-TiO_2 samples was evaluated by the degradation of methyl orange. Comparing to the undoped TiO_2, 6% Cu-TiO_2 sample exhibited remarkably high photocatalytic towards methyl orange under simulated sunlight irradiation, which was attributed to the fact that copper ion doping produced numerous oxygen vacancies (V_O) in the material. In addition, it also showed improved antibacterial properties against both Gram-positive Staphylococcus aureus (*S.aureus*) and Gram-negative Escherichia coli (*E.coli*) bacteria. These results establish that Cu^{2+} doping can obviously improve the photocatalytic performance of TiO_2 under simulated sunlight.

1. Introduction: Photocatalytic degradation of pollutants using solar energy is a green and sustainable strategy to solve energy crisis and environmental problems [1–3]. Over the past decades, inorganic semiconductor materials have been extensively investigated for photocatalytic degradation of pollutants [4–6]. Specifically, TiO_2 was found to be the most efficient and low-cost inorganic semiconductor photocatalysts due to its high chemical stability, outstanding mechanical, catalytic, and optical properties [7–9]. In fact, it has shown high catalytic activity and unique selectivity in many catalytic reactions. However, the wide-bandgap energy of TiO_2 (~ 3.2 eV) limits its widespread use as photocatalyst under sunlight because previous studies have illustrated that only less than 5% UV radiations of the solar spectrum can be utilised by TiO_2 [10–12]. Therefore, it is of great importance to improve the photocatalytic performance of TiO_2 for use in pollutant degradation under sunlight.

Recently, in order to make TiO_2 better use of the solar spectrum, several approaches, such us precious metal deposition, non-metallic or metallic elements doping, and semiconductor coupling, have been developed to deal with the insufficient of TiO_2 material [13–17]. Among them, element doping with metals and non-metals is considered as the simplest and inexpensive way. For example, Julien G. Mahy *et al.* [16] investigated the degradation activity of N-doped TiO_2 catalysts on p-nitrophenol, and the results showed that N-doped catalysts had a significantly improved degradation capability under visible light. Shafei and Sheibani [18] reported the preparation of Cu-doped TiO_2-CNT nanocomposite powder and found that the catalyst exhibited great efficiency in the degradation rate of methylene blue under visible-light irradiation. Bing Liu *et al.* [19] have prepared mulberry shaped TiO_2-Au nanocomposite via a one-step hydrothermal method, and they found that TiO_2-Au nanocomposite showed excellent photocatalytic performance for efficient H_2 generation under visible light. In the last few decades, great progress had been made in producing TiO_2 photocatalytic materials, either, too low light conversion efficiency or too expensive limit their further application. Therefore, it is extremely appealing to develop the modified TiO_2 photocatalysts that combine low-cost and excellent energy conversion efficiency. In addition, although some papers about Cu-doped TiO_2 have been published in the literature [20], there has been little research on the photocatalytic mechanism of Cu-doped TiO_2.

Here, a facile hydrothermal method to synthesise Cu-TiO_2 samples with a controllable crystal phase, excellent methyl orange (MO) removal capacity, and enhanced antimicrobial activity, is reported. Notably, the 6% Cu-TiO_2 sample showed distinctly enhanced photocatalytic performance than corresponding undoped TiO_2 sample. X-ray powder diffraction (XRD) and Raman spectra revealed that Cu^{2+} ion was doped into TiO_2 crystal lattice and abundant oxygen vacancies were thus generated. We concluded that these oxygen vacancies increased the number of active sites in TiO_2 sample and improved the catalytic performance and antimicrobial activity of the TiO_2 sample in the end.

2. Experimental

2.1. Reagents and materials: Titanium sulfate ($Ti(SO_4)_2$), ethylenediaminetetraacetic acid (EDTA), copper chloride dihydrate ($CuCl_2{\cdot}2H_2O$), and ethanol were obtained from Aladdin Chemical Reagent Co., Ltd. All chemicals were analytical-grade reagents and used as received without further purification.

2.2. Synthesis of (0, 2, 4, 6, 8, and 10%) Cu-TiO_2 hollow spheres: $Ti(SO_4)_2$ (0.2400 g) and EDTA (1.4610 g) were dispersed in deionised water (30 ml) under magnetic stirring for 15 min at room temperature. Then, a specific amount of $CuCl_2{\cdot}2H_2O$ (calculated according to the molar ratio of $CuCl_2{\cdot}2H_2O$ to Ti $(SO_4)_2$) was added with vigorous stirring for 15 min. The obtained mixture suspensions were transferred into a 50 ml autoclave and reacted at 180°C for 8 h. After cooling to room temperature naturally, the resulting powders were collected and washed repeatedly with deionised water and ethanol for three times. Finally, the Cu-TiO_2 samples were dried at 80°C for 12 h in air.

2.3. Characterisation: XRD data were collected on an XRD-6000 X-Ray diffractometer (Shimadzu) using Cu Kα radiation ($\lambda = 0.15405$ nm). Microstructure was observed on a scanning electron microscope (SEM) (Hitachi, S-4800) and a transmission electron microscope (TEM) (FEI, Tecnai G2 S-Twin). Raman spectra of the samples were measured with the Renishaw inVia Reflex spectrometer system. The UV–Vis absorption spectrum was performed by using a UV–Vis spectrophotometer (U-4100, Hitachi, Japan) in the region of 200–800 nm. Electron paramagnetic resonance (EPR) spectra were obtained on a Bruker 500

spectrometer at 90 K. X-ray photoelectron spectroscopy (XPS) measurements were conducted on a Leybold-Heraeus LHS-10 spectrometer.

2.4. Photocatalytic activity measurements: The photocatalytic performances of the samples were tested by degradation of MO under simulated sunlight irradiation. In each experiment, 10 mg photocatalyst was added into a 20 mg/l MO aqueous solution (40 ml). pH of the mixed solution was adjusted to 5.5 using 0.1 M sodium hydroxide (NaOH) solution and 0.1 M hydrochloric acid (HCl) solution. Then the suspension was continuously stirred for 60 min in the dark to ensure that the MO accomplished adsorption–desorption equilibrium. A 300 W Xe lamp (Microsolar300, Beijing Prefect Light) was used as simulated sunlight source, irradiating atop 15 cm distance away from the beaker containing photocatalyst and MO aqueous solution. At defined irradiation intervals, about 3 ml of the solution was sampled and filtered through a 0.24 mm membrane. The concentration of MO was analysed by a PGENERAL TU-1901 UV–Vis spectrophotometer. The 6% Cu-TiO_2 sample was repeatedly used for three times under the same experiment conditions to test the photocatalytic stability.

2.5. Bacterial preparation: *S. aureus* (ATCC6538) and *E. coli* (ATCC25922) were used as a Gram-positive and Gram-negative bacterium, respectively. Bacteria were cultured on nutrient agar (*Difco*) for 24 h at 37 °C. The subcultured bacteria were washed and resuspended in the nutrient broth (*Difco*). The required concentration of inoculum was adjusted to 10^7 cfu·ml^{-1} using the McFar-land scale.

2.6. Antibacterial property: Radial diffusion method was used to investigate the antibacterial activities of the 6%Cu-TiO_2 sample on the growths of the Gram-positive (*S. aureus*) and Gram-negative (*E. coli*). Firstly, the pre-prepared sterile paper was placed in a suspension of Cu-TiO_2 (0.1 g/l), fully soaked and then dried. The sterilisation extract agar medium covered the whole bottom of the culture dish about 3 mm thick. The two bacteria (about 10^7 cfu·ml^{-1}) were evenly spread to form a uniform membrane on the surface of the agar. Then place the papers with the sample on the surface of the agar plate. The dishes sealed by para-film were exposed to simulated sunlight for 2 h, then cultured at 37° C for 24 h. The diameters of bacteriostatic rings were measured with Vernier caliper. All the experiments were repeated for three times. The control experiments were performed in total darkness.

3. Results and discussion

3.1. Crystal structure: The XRD patterns of the as-synthesised TiO_2 hollow spheres with different Cu^{2+} ion doping concentrations were given in Fig. 1*a*. As we can see from Fig. 1*a*, XRD diffraction peaks of all samples were consistent with the standard card (PDF#21-1272) of pure anatase phase and no miscellaneous peaks were detected, illustrating that Cu^{2+} ion had been successfully incorporated into the TiO_2 crystal structure. The average crystal size for each sample, calculated according to the Scherrer equation, was 11.59, 11.82, 12.28, 12.78, 15.61, and 15.79 nm for the 0% Cu-TiO_2, 2% Cu-TiO_2, 4% Cu-TiO_2, 6% Cu-TiO_2, 8% Cu-TiO_2, and 10% Cu-TiO_2, respectively. It can be found that the crystallite size of the samples gradually increased with increasing Cu content from 0 to 10%. Furthermore, the intensity of the XRD diffraction peaks was found to have decreased with an increase in Cu content, which might be because the doping of Cu^{2+} ion changed the cell volume and reduced the crystallinity of the TiO_2 sample. As shown in Fig. 2, abundant oxygen vacancies were generated by Cu^{2+} ion to occupy the position of Ti^{4+} ion because of Jahn–Teller distortions. In addition, with the increasing molar ratio of Cu^{2+} ion, the diffraction peak at 25.3° gradually shifted to larger 2θ angles because of the introduction of lattice strain (Fig. 1*b*).

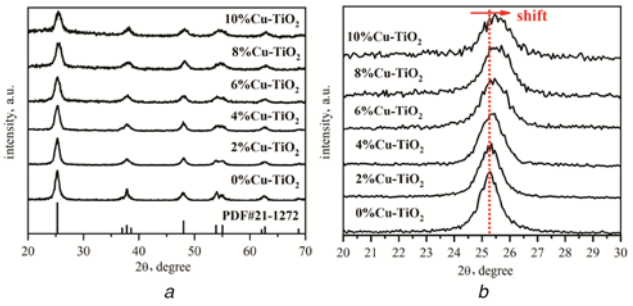

Fig. 1 *XRD patterns of various Cu-TiO_2 samples*
a Cu content from 0 to 10%
b Enlarged view of XRD patterns of X% Cu-TiO_2 samples (X = 0, 2, 4, 6, 8, 10)

3.2. Raman spectra analysis: The lattice perturbations in the local structure of the TiO_2 samples with different Cu doping concentrations were characterised by Raman spectroscopy (Fig. 3). Obviously, the Raman spectra results showed that the phase compositions of all samples were almost consistent with the XRD results. As shown in Fig. 3*a*, all samples showed four obvious peaks at 146.9, 397.3, 512.3, and 638.5 cm^{-1}, which could be assigned to the characteristic $E_{g(1)}$, B_{1g}, A_{1g}, and $E_{g(3)}$ vibration modes of the anatase TiO_2 [21], respectively. No peaks of any copper-related impurities were detected, further suggesting the successful doping of Cu^{2+} ion into the TiO_2 lattice. Furthermore, as the amount of Cu dopant was increased from 0 to 10% (Fig. 3*b*), the $E_{g(1)}$ peak shifted to higher frequencies, which indicated that new Cu–O bonds and abundant V_O had been formed.

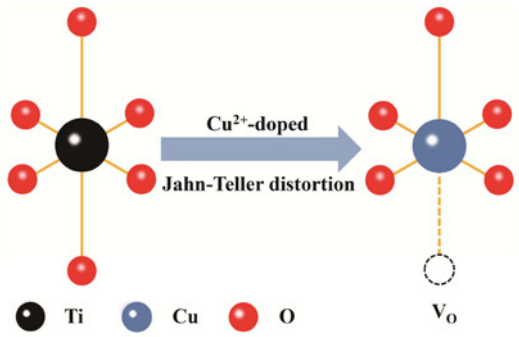

Fig. 2 *Process of oxygen-vacancy formation in TiO_2*

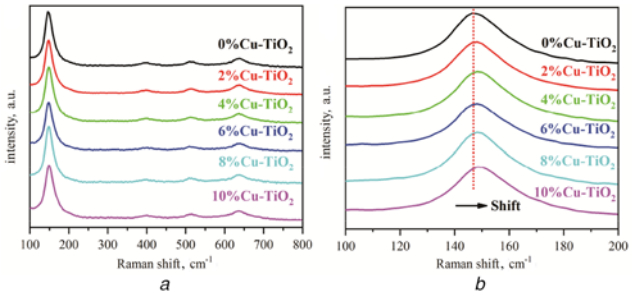

Fig. 3 *Raman spectra of the TiO_2 samples with different Cu doping concentrations*
a Cu content from 0 to 10%
b Enlarged view of Raman spectra of X% Cu-TiO_2 samples (X = 0, 2, 4, 6, 8, 10)

doi: 10.1049/mnl.2019.0781

3.3. Morphology: Fig. 4 shows typical SEM and TEM images of pure TiO_2 and 6% Cu-TiO_2 samples. The SEM image indicated that the pure TiO_2 sample was composed of irregular microsphere in diameter ranging from 0.5 to 1 μm (Fig. 4*a*). Moreover, it was observed that many nanoparticles were distributed on the surface of TiO_2 microsphere. From the TEM results (Fig. 4*c*), the TiO_2 sample showed a hollow microsphere structure, and some nanoparticles were anchored on the surface, which was consistent with the SEM image. When Cu ion was successfully doped into TiO_2 lattice (Fig. 4*b*), no significant morphology change was observed, demonstrating the excellent structural stability of TiO_2 hollow spheres. TEM image of 6% Cu-TiO_2 sample displayed in Fig. 4*d* further revealed that the hollow structure of the samples did not change (Fig. 4*d*).

3.4. Photocatalytic performance: The photocatalytic performances of different TiO_2 hollow spheres were evaluated using MO as the probe molecule under simulated sunlight irradiation. Fig. 5*a* shows the degradation efficiency curves of MO. The control experiment showed that no MO solution was degraded without catalyst under analogous experimental conditions. In addition, because of the large bandgap and weak photoresponse of TiO_2 samples studied, the photocatalytic activity demonstrated here was low. As Cu^{2+} ion was introduced into TiO_2, all samples exhibited remarkably enhanced photocatalytic ability. Thus, it can be inferred that oxygen vacancies play key roles in efficient removal of MO pollutants. Specifically, it can be seen that 6% Cu-TiO_2 hollow spheres had the best photocatalysis activity and MO molecules were completely degraded after 15 min simulated sunlight irradiation. This suggested that the optimum molar ratio of the Cu^{2+} to TiO_2 was 6%. Furthermore, the photocatalytic degradation efficiencies of MO corresponding to the different photocatalysts followed the sequence: 6% Cu-TiO_2 > 4% Cu-TiO_2 > 8% Cu-TiO_2 > 2% Cu-TiO_2 > 10% Cu-TiO_2 > TiO_2. However, we can see that a large excess of Cu^{2+} doping content resulted in a great decrease in the degradation efficiency of MO, which should be ascribed to the formation of extra phases that they were located on the surface of TiO_2 hollow microspheres and covered the active sites of catalytic reactions.

The first-order equation ($\mathrm{Ln}(C/C_0) = -kt$) was adopted to describe the above photocatalytic experimental data, where k is the reaction rate constant. As shown in Fig. 5*b*, the calculated reaction rate constants were 0, 0.028, 0.044, 0.093, 0.208, 0.055, and 0.034 min^{-1} for blank sample, and Cu-TiO_2 hollow spheres with a copper ion doping concentration from 0 to 10%, respectively. It can be seen that the 6% Cu-TiO_2 photocatalyst had the maximum photodegradation rate constant to MO, which was about 7.4 times higher than that of undoped TiO_2 sample. The above results further demonstrated that introducing oxygen vacancies was crucial for improving the photocatalytic activity of TiO_2.

3.5. Stability test and optical characteristics: To verify the stability of the photocatalyst, the recycling experiments about MO photodegradation were performed with 6% Cu-TiO_2 catalyst. As can be seen from Fig. 6*a*, when the experiments were repeated once, the activity of photocatalyst was basically unchanged. After three cycles, about 87.7% of MO was degraded. The above results demonstrated that 6% Cu-TiO_2 catalyst had an excellent stability. UV–Vis absorption spectra were measured to investigate the optical properties of the TiO_2 samples with different Cu doping concentrations (Fig. 6*b*). Obviously, it can be seen that the pure TiO_2 hollow spheres presented intense absorption in the ultraviolet domain ($\lambda < 400$ nm) and weak absorption in the visible region ($\lambda \geq 400$ nm). Compared with pure TiO_2, after introducing oxygen vacancy through Cu^{2+} doping, the UV–Vis absorption spectrum of Cu-TiO_2 hollow spheres showed a significant red-shift, which indicated the sample can capture more visible light to produce more photo-generated electron–hole pairs, therefore ensuring the high light utilisation efficiency. As a result, the photocatalytic activity of Cu-TiO_2 samples was greatly improved. It should be noted that all the Cu-TiO_2 samples showed strong absorption in the near-infrared region (ca. 800 nm), which was due to d–d transitions of the dopant Cu^{2+} ion [22].

3.6. EPR and XPS analyses: The microstructures of TiO_2 and 6% Cu-TiO_2 samples were further studied by EPR and XPS analyses. As shown in Fig. 7*a*, TiO_2 sample did not exhibit a detectable EPR signal. Compared to pure TiO_2 sample, an EPR signal with the g factor of 2.39 appeared after doping Cu^{2+} ion, which was

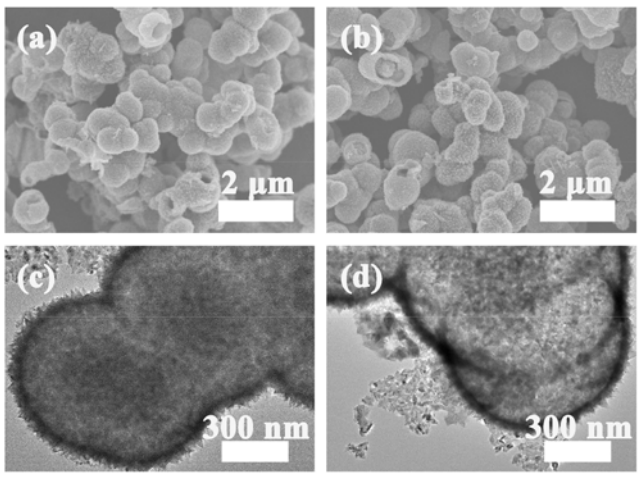

Fig. 4 *SEM and TEM images of*
a, c TiO_2 hollow spheres
b, d Cu-TiO_2 hollow spheres

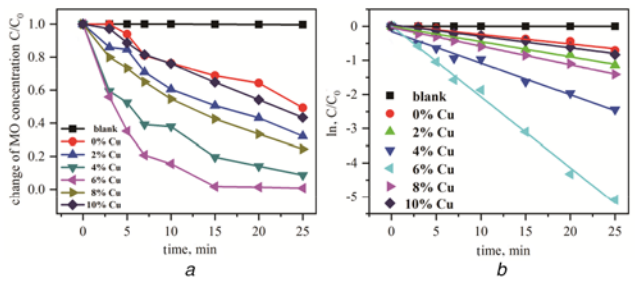

Fig. 5 *Photocatalytic degradation curves of MO solution*
a Photocatalytic degradation rate of MO under simulated sunlight irradiation of all the synthesised samples
b First-order kinetic curves of all samples

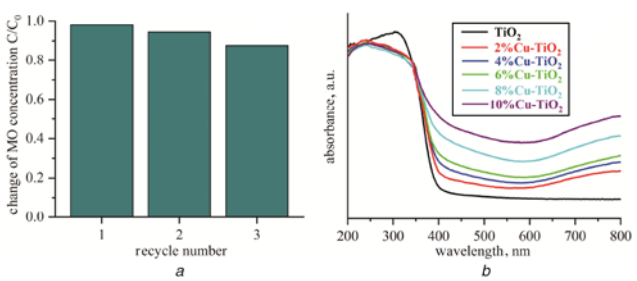

Fig. 6 *Stability test and optical absorption spectra*
a Recycle test of photodegradation of MO over 6% Cu-TiO_2 photocatalyst
b UV–Vis absorption spectra of the TiO_2 samples with different Cu doping concentrations

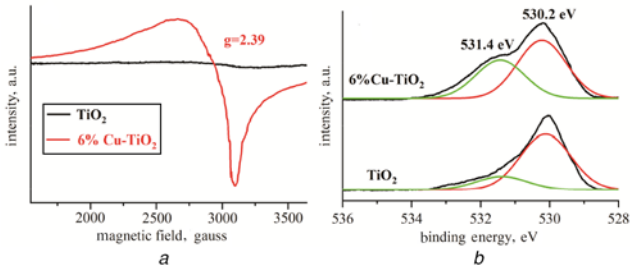

Fig. 7 *EPR and XPS spectra of TiO_2 and 6% Cu-TiO_2*
a EPR spectra
b High resolution O 1s XPS spectra of TiO_2 and 6% Cu-TiO_2

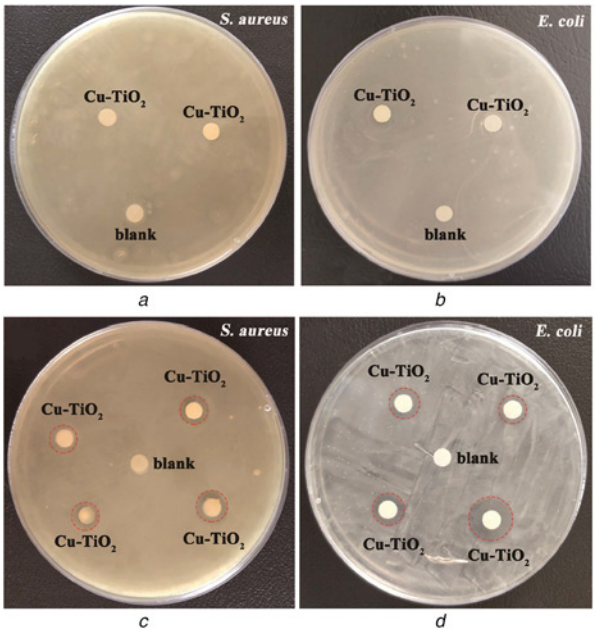

Fig. 8 *Zone of inhibition of 6% Cu-TiO_2 hollow spheres against S. aureus and E.coli*
a, b In total darkness
c, d With light irradiation for 2 h

consistent with an octahedral coordination of Cu^{2+} ion [23]. This conclusion further showed that Cu^{2+} ion had successfully occupied the position of Ti^{4+} ion. In order to prove that abundant oxygen vacancies were generated in the as-prepared 6% Cu-TiO_2 sample, we performed O 1s XPS measurements for TiO_2 and 6% Cu-TiO_2 samples (Fig. 7*b*). The peak at about 531.4 eV corresponds to the oxygen vacancies in the matrix of TiO_2, and the peak at 530.2 eV originates from the oxygen bond of Ti–O–Ti [24]. Interestingly, the peak area of oxygen vacancies significantly increased in the 6% Cu-TiO_2 sample in comparison with the pure TiO_2 sample. This indicated that abundant oxygen vacancies were generated as Cu^{2+} ion was substituted for Ti^{4+} ion site.

3.7. Antimicrobial activity: In order to better evaluate the photocatalytic behaviour of 6% Cu-TiO_2 sample, antimicrobial activity test was further detected. Fig. 8 shows the results obtained by inhibition ring method. In the control group, no inhibition zones were detected (Figs. 8*a* and b). However, when the dishes were illuminated by simulated sunlight, 6% Cu-doped TiO_2 sample exhibited obvious inhibition zones (Figs. 8*c* and 8*d*), indicating that the 6% Cu-TiO_2 hollow spheres had strong antibacterial activity against both *S. aureus* and *E. coli*. The average width of the inhibition zone of the 6% Cu-TiO_2 samples on *S. aureus* and

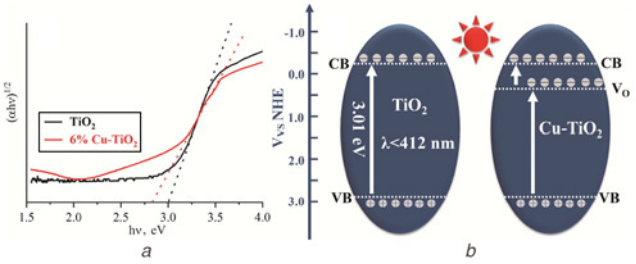

Fig. 9 *Tauc plots and schematic diagram of the photocatalytic mechanism*
a Plots of $(ahv)^{1/2}$ versus photon energy (hv) for pure TiO_2 and 6% Cu-TiO_2 samples
b Illustration of photocatalytic mechanism

E. coli was 8.21 and 9.57 mm, respectively. Compared with the data given in the literature [25–28], our sample had better antibacterial effect. What is more, the 6% Cu-TiO_2 sample showed higher antimicrobial activity towards *E. coli* than *S. aureus*, which was attributed to the different chemical composition of the cell surfaces [29].

3.8. Photocatalytic mechanism: As is well known, the photocatalytic activity of TiO_2 is closely related to its optical bandgap. The bandgap energy of pure TiO_2 and 6% Cu-TiO_2 samples were determined from the extrapolation of Tauc plots of $(h\nu\alpha)^{1/2}$ as a function of photon energy ($h\nu$) and the obtained results were shown in Fig. 9*a*. Clearly, the bandgap energy (E_g) of pure TiO_2 was ca. 3.01 eV. However, the E_g of the Cu^{2+}-doped TiO_2 sample decreased to 2.82 eV. Based on above experimental results, a possible photocatalytic mechanism was proposed (Fig. 9*b*). In contrast to pure TiO_2 sample, 6% Cu-TiO_2 sample showed an enhanced response to visible light because oxygen vacancies generated by doping Cu^{2+} ion reduced the bandgap of TiO_2 [24]. Furthermore, oxygen vacancies also played photogenerated charges traps and adsorption sites roles in photocatalytic reaction, which was favourable for the transfer of photogenerated charges and the exposure of active sites [30]. Therefore, the photocatalytic activity of 6% Cu-TiO_2 sample was greatly improved.

4. Conclusion: In summary, we developed a new strategy to prepare Cu-doped TiO_2 samples with abundant oxygen vacancies by a convenient hydrothermal method. The optimal Cu^{2+} concentration was found to be 6 mol% relative to the amount of TiO_2, and the Cu^{2+}-doped did not affect the crystal phase of TiO_2 or the particle morphologies. The significant improvement in MO removal and antimicrobial activity is mainly due to the generation of numerous oxygen vacancies and optical properties of 6% Cu-TiO_2 samples. Consistent with the prior studies, our study indicated that the oxygen vacancies played an important role in improving the photocatalytic efficiency of TiO_2. This material can be used as a potential antibacterial agent in biomedical materials and a pollutant treatment agent in the environmental industry. Furthermore, it can also be used for food packaging material in the food industry.

5. Acknowledgments: This work was supported by the Science and Technology Plan Project of Qiqihar City (grant SFGG-201702).

6 References

[1] Xiao Y., Tao X.Q., Qiu G.H., *ET AL.*: 'Optimal synthesis of a direct Z-scheme photocatalyst with ultrathin $W_{18}O_{49}$ nanowires on G-C_3N_4 nanosheets for solar-driven oxidation reactions', *J. Colloid Interface Sci.*, 2019, **550**, pp. 99–109
[2] Li X.B., Xiong J., Gao X.M., *ET AL.*: 'Recent advances in 3d G- C_3N_4 composite photocatalysts for photocatalytic water splitting, degradation of pollutants and CO_2 reduction', *J. Alloys Compd.*, 2019, **802**, pp. 196–209

doi: 10.1049/mnl.2019.0781

[3] Qian X.F., Xu H., Zhang X., *ET AL.*: 'Enhanced visible-light-driven photocatalytic activity of Ag_3PO_4/metal-organic framework composite', *Polyhedron*, 2019, **163**, pp. 1–6

[4] Tang Y.X., Zhang X., Ma Y.X., *ET AL.*: 'One-dimensional core-shell $Zn_{0.1}Cd_{0.9}S/Snln_4S_8$ heterojunction for enhanced visible light photocatalytic degradation', *Sep. Purif. Technol.*, 2020, **230**, p. 115896

[5] Selvaraj S., Mohan M.K., Navaneethan M., *ET AL.*: 'Synthesis and photocatalytic activity of Gd doped ZnO nanoparticles for enhanced degradation of methylene blue under visible light', *Mater. Sci. Semicond. Process.*, 2019, **103**, p. 104622

[6] Rosaline D.R., Inbanathan S.S.R., Suganthi A., *ET AL.*: 'Visible-light driven photocatalytic degradation of eosin yellow (Ey) dye based on nio-Wo3 nanoparticles', *J. Nanosci. Nanotechnol.*, 2020, **20**, (2), pp. 924–933

[7] Li F., Lu C., Xu B., *ET AL.*: 'Photocatalytic degradation of rhodamine B under visible light irradiation by TiO_2 doped layered zirconium phosphates', *J. Nanosci. Nanotechnol.*, 2020, **20**, (3), pp. 1697–1703

[8] Diaz-Uribe C.E., Rodriguez A., Utria D., *ET AL.*: 'Photocatalytic degradation of Methylene blue by the anderson-type polyoxomolybdates/TiO_2 thin films', *Polyhedron*, 2018, **149**, pp. 163–170

[9] Koohestani H.: 'Photocatalytic removal of cyanide and Cr(Iv) from wastewater in the presence of each other by using TiO_2/UV', *Micro Nano Lett.*, 2019, **14**, (1), pp. 45–50

[10] Li B.X., Hao Y.G., Zhang B.S., *ET AL.*: 'A multifunctional noble-metal-free catalyst of CuO/TiO_2 hybrid nanofibers', *Appl. Catalysis A-Gen.*, 2017, **531**, pp. 1–12

[11] Fan J.M., Lei Y.Y., Gu Z.Y., *ET AL.*: 'Fabrication of N and F modified La-TiO_2 nanoparticles and their enhanced photocatalytic response to visible light', *J. Nanosci. Nanotechnol.*, 2020, **20**, (2), pp. 779–788

[12] Mutyala S., Sadiq M.M.J., Gurulakshmi M., *ET AL.*: 'Disintegration of flower-like MoS_2 to limply allied layers on spherical nanoporous Tio2: enhanced visible-light photocatalytic degradation of methylene blue', *J. Nanosci. Nanotechnol.*, 2020, **20**, (2), pp. 1118–1129

[13] Umar K., Parveen T., Khan M.A., *ET AL.*: 'Degradation of organic pollutants using metal-doped TiO_2 photocatalysts under visible light: a comparative study', *Desalin. Water Treat.*, 2019, **161**, pp. 275–282

[14] Pedroza-Herrera G., Medina-Ramírez I.E., Lozano-Álvarez J.A., *ET AL.*: 'Evaluation of the photocatalytic activity of copper doped TiO_2 nanoparticles for the purification and/or disinfection of industrial effluents', *Catal. Today*, 2020, **341**, pp. 37–48

[15] Chen Y., Wu Q., Wang J., *ET AL.*: 'Self-floating Cu/N Co-doped TiO_2/diatomite granule composite with enhanced visible-light-responsive photoactivity and reusability', *J. Chem. Technol. Biotechnol.*, 2019, **94**, (4), pp. 1210–1219

[16] Mahy J.G., Cerfontaine V., Poelman D., *ET AL.*: 'Highly efficient low-temperature N-doped TiO_2 catalysts for visible light photocatalytic applications', *Materials*, 2018, **11**, (4), p. 584

[17] Wang S.M., Yan X.X., Deng D.M., *ET AL.*: 'Controllable synthesis and enhanced photocatalytic activity of B-TiO_2 nanospheres', *Micro Nano Lett.*, 2019, **14**, (7), pp. 740–743

[18] Shafei A., Sheibani S.: 'Visible light photocatalytic activity of Cu doped TiO_2-Cnt nanocomposite powder prepared by Sol–Gel method', *Mater. Res. Bull.*, 2019, **110**, pp. 198–206

[19] Liu B., Wang Y., Shang S.X., *ET AL.*: 'One-step synthesis of mulberry-shaped TiO_2-Au nanocomposite and its H_2 evolution property under visible light', *Colloids Surf. A, Physicochem. Eng. Asp.*, 2018, **553**, pp. 203–209

[20] Liu J., Li X.-M., He J., *ET AL.*: 'Combining the photocatalysis and absorption properties of core-shell Cu-btc@TiO_2 microspheres: highly efficient desulfurization of thiophenic compounds from fuel', *Materials*, 2018, **11**, (11), p. 2209

[21] Ceballos-Chuc M.C., Ramos-Castillo C.M., Alvarado-Gil J.J., *ET AL.*: 'Influence of brookite impurities on the Raman Spectrum of TiO_2 anatase nanocrystals', *J. Phys. Chem. C*, 2018, **122**, (34), pp. 19921–19930

[22] Colón G., Maicu M., Hidalgo M.C., *ET AL.*: 'Cu-doped TiO_2 systems with improved photocatalytic activity', *Appl. Catal., B*, 2006, **67**, (1-2), pp. 41–51.

[23] Kucherov A.V., Slinkin A.A.: 'Introduction of transition metal ions in cationic positions of high-Silica Zeolites by a solid state reaction. Interaction of copper compounds with H-mordenite or H-zsm-5', *Zeolites*, 1986, **6**, (3), pp. 175–180

[24] Li J., Zhang M., Guan Z., *ET AL.*: 'Synergistic effect of surface and bulk single-electron-trapped oxygen vacancy of TiO_2 in the photocatalytic reduction of CO_2', *Appl. Catal., B*, 2017, **206**, pp. 300–307

[25] Xue X., Wang Y., Yang H.: 'Preparation and characterization of boron-doped titania nano-materials with antibacterial activity', *Appl. Surf. Sci.*, 2013, **264**, pp. 94–99

[26] Jin W., Li J., Zhuang X.-W., *ET AL.*: 'Improved mould resistance and antibacterial activity of Bamboo coated with ZnO/Graphene', *R. Soc. Open Sci.*, 2018, **5**, (8), p. 180173

[27] Xue C.H., Chen J., Yin W., *ET AL.*: 'Superhydrophobic conductive textiles with antibacterial property by coating fibers with silver nanoparticles', *Appl. Surf. Sci.*, 2012, **258**, (7), pp. 2468–2472

[28] Wang Y., Xue X., He Y.J.V.: 'Modification of the antibacterial activity of Zn/TiO_2 nano-materials through different anions doped', *Vacuum*, 2014, **101**, pp. 193–199

[29] Podporska-Carroll J., Panaitescu E., Quilty B., *ET AL.*: 'Antimicrobial properties of highly efficient photocatalytic TiO_2 nanotubes', *Appl. Cataly. B, Environ.*, 2015, **176**, pp. 70–75

[30] Feng X., Wang P., Hou J., *ET AL.*: 'Significantly enhanced visible light photocatalytic efficiency of phosphorus doped TiO_2 with surface oxygen vacancies for ciprofloxacin degradation: synergistic effect and intermediates analysis', *J. Hazard. Mater.*, 2018, **351**, pp. 196–205